第125巻　第５号　平成29年５月１日発行（毎月1回1日発行）　ISSN 1348-6535 CODEN:JCSJEW

JCS-Japan

June

vol.125

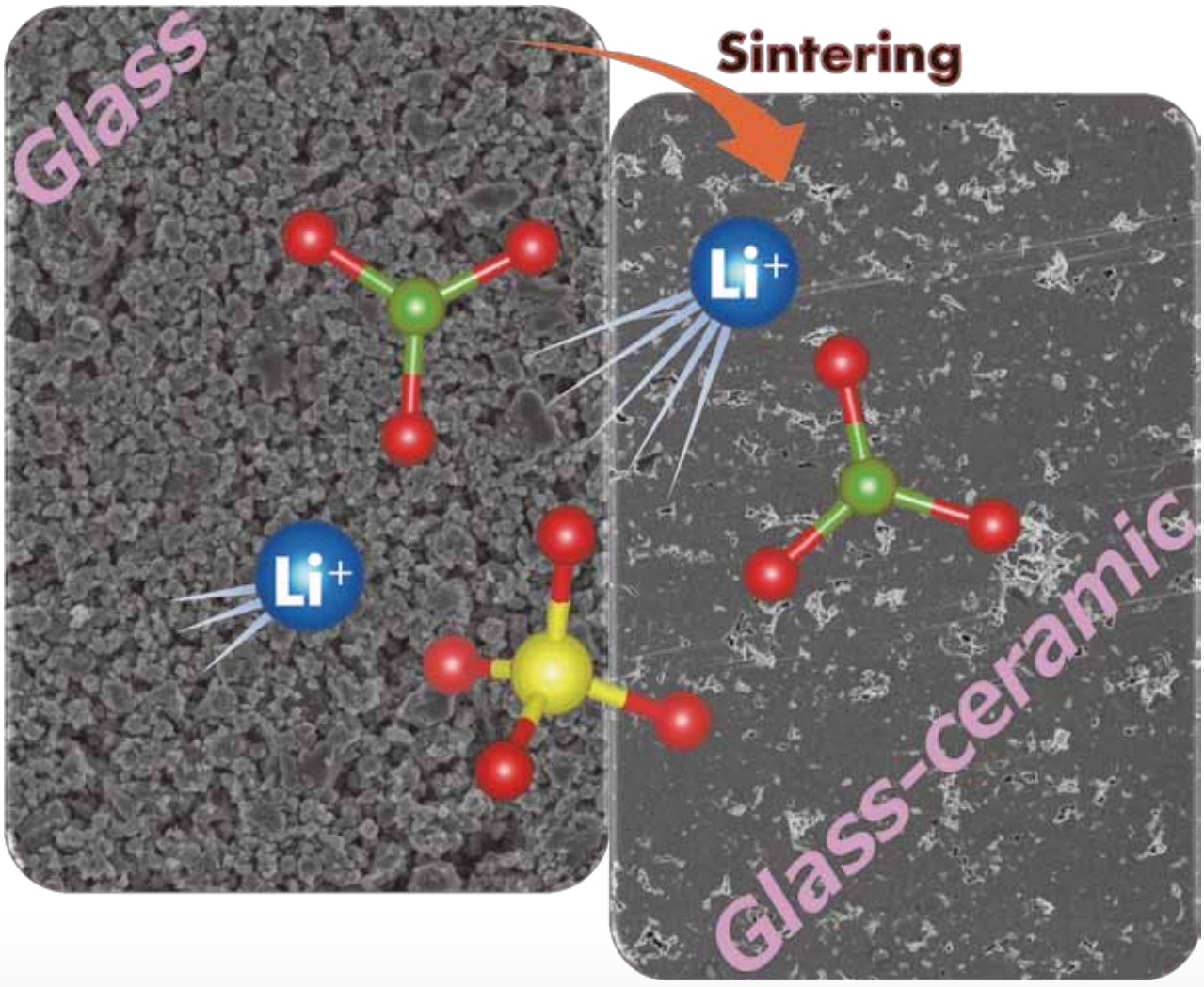

Journal of the Ceramic Society of Japan

2017

Journal of the Ceramic Society of Japan 125 [6] 433-437 2017 Full paper

Electrical and mechanical properties of glass and glass-ceramic electrolytes in the system Li_3BO_3–Li_2SO_4

Masahiro TATSUMISAGO†, Ryohei TAKANO, Masashi NOSE, Kenji NAGAO, Atsutaka KATO, Atsushi SAKUDA*, Kiyoharu TADANAGA and Akitoshi HAYASHI**

Department of Applied Chemistry, Graduate School of Engineering, Osaka Prefecture University, 1–1 Gakuen-cho, Naka-ku, Sakai 599–8531, Japan

***Department of Energy and Environment, Research Institute of Electrochemical Energy, National Institute of Advanced Industrial Science and Technology (AIST), 1–8–31 Midorigaoka, Ikeda, Osaka 563–8577, Japan**

****Department of Materials Chemistry, Faculty of Engineering, Hokkaido University, Sapporo 060–8628, Japan**

Low-melting oxide glasses are promising as electrolytes for all-solid-state lithium rechargeable batteries. Glasses in the pseudobinary system Li_3BO_3–Li_2SO_4 were prepared by a mechanochemical technique. Raman spectra revealed that the glasses contained no macroanions which form networks but consisted only of Li^+ ions and two discrete ortho-oxoanions, BO_3^{3-} and SO_4^{2-}. The density and molar volume increased and elastic moduli decreased with an increase in the Li_2SO_4 content in the glasses. The heat treatment of the Li_3BO_3–Li_2SO_4 glasses at around 300°C brought about the crystallization to form ion conducting glass-ceramics. Electrical conductivities of the glasses and glass-ceramics in this system were maximized with the mixing of Li_3BO_3 and Li_2SO_4. The conductivities were higher in the glass-ceramics of the compositions with small amounts of Li_2SO_4, ranging from 3×10^{-6} to 1×10^{-5} S cm^{-1} at room temperature, compared to the corresponding glasses. This conductivity enhancement by the heat treatment is probably due to the precipitation of solid solutions with a high temperature Li_3BO_3 phase.

Key-words : Solid electrolyte, Ionic glass, Glass-ceramic, All-solid-state battery

[Received February 13, 2017; Accepted March 28, 2017]

1. Introduction

Glass-based solid electrolytes with high lithium-ion conductivity have been gaining much attention because of their potential application to safe and reliable all-solid-state lithium rechargeable batteries.[1] Sulfide glasses[2] and glass-ceramics[3),4] are promising for these batteries because of their high ionic conductivities around 10^{-2} S cm^{-1} at room temperature[4] comparable to organic liquid electrolytes and superionic sulfide crystals.[5] Sulfide glass-based electrolytes have a great advantage in achieving close solid/solid contacts by just a cold-press without high-temperature sintering because of their excellent formability at room temperature.[6] A disadvantage of sulfide electrolytes is their instability under regular air atmosphere with moisture. Oxide-based solid electrolytes, on the other hand, are favorable for battery application because of their high stability in air atmosphere with no possibility of H_2S gas generation from the electrolytes. However, it is very hard to use oxide solid electrolytes in all-solid-state batteries mainly because they have quite poor deformability at room temperature, and thus there remains large interfacial resistance between electrolytes and electrodes.[6] A sintering process of oxide electrolytes at high temperatures sometimes causes chemical reactions at the interface between electrolytes and electrodes to cause the large interfacial resistances. To obtain excellent oxide solid electrolytes suitable for application in all-solid-state rechargeable batteries, "low melting" is one of the most important properties.

A series of mixed-former glasses with high lithium ion conductivity were reported in lithium ortho-oxosalt pseudobinary systems such as Li_4SiO_4–Li_3BO_3.[7] Various kinds of mixed-former "ion glasses" as oxide solid electrolytes were developed by using rapid melt-quenching and mechanochemical techniques.[8),9] The Li_3BO_3–Li_2SO_4 glassy system, one of these ion glass systems, is most attractive in the sense of low melting character. In addition, since both Li_3BO_3 and Li_2SO_4 have superionic high-temperature phases,[10),11] these superionic phases could precipitate during glass heating to obtain highly conductive glass-ceramic electrolytes.[3] So we tried to evaluate the possibility of the Li_3BO_3–Li_2SO_4 glass and glass-ceramic materials as an excellent oxide solid electrolyte for the application to all-oxide battery systems.

Recently we have successfully prepared highly conductive and low-temperature deforming $Li_{2.9}B_{0.9}S_{0.1}O_{3.1}$ ($90Li_3BO_3 \cdot 10Li_2SO_4$ in mol%) glass-ceramics.[12] Our previous paper mainly reported the characterization and the application of these newly obtained glass-ceramics to oxide-based all-solid-state lithium secondary batteries using conventional electrode active materials.[12] The present paper reports physicochemical properties and structure of the mechanochemically prepared Li_3BO_3–Li_2SO_4 glasses. Mechanical, electrical and thermal properties and densities were examined for the binary glasses in a wide range of composition. The formation and characterization of heat-treated glass-ceramics were done on the basis of the diffraction and conductivity measurements.

2. Experimental

The Li_3BO_3–Li_2SO_4 glasses were prepared by a mechanochemical technique using Li_3BO_3 and Li_2SO_4 crystals. The Li_3BO_3 crystal was prepared by heating a mixture of $LiOH \cdot H_2O$ (>99%; Wako Chem.) and H_3BO_3 (>99%; Wako Chem.) at 500°C for 1 h and then sintering the product at 600°C for 2 h in

† Corresponding author: M. Tatsumisago; E-mail: tatsu@chem.osakafu-u.ac.jp

DOI http://doi.org/10.2109/jcersj2.17026

air. The Li_2SO_4 crystal was prepared by heating $Li_2SO_4 \cdot H_2O$ (>99%; Aldrich Chem.) at 300°C for 2 h under Ar atmosphere. A mixture of the crystals of Li_3BO_3 and Li_2SO_4 was put into a 45 ml ZrO_2 pot with 500 ZrO_2 balls (5 mm in diameter) and milled at the rotating speed of 370 rpm and the milling periods of 40–144 h. A planetary ball mill apparatus (Pulverisette 7, Fritsch GmbH) was used. All processes were conducted in a dry Ar atmosphere. Glass-ceramic samples were prepared by heating the glass samples.

X-ray diffraction (XRD) measurements (Cu Kα) were conducted using a diffractometer (SmartLab, Rigaku Corp.) to identify crystal phases of the glass samples and the glass-ceramic samples. Differential thermal analyses (DTA) were performed using a thermal analyzer (Thermo-plus 8120, Rigaku Corp.) to observe glass-transition, crystallization and melting temperatures. The mechanochemically prepared samples, which were sealed in Al pans in an Ar-filled glove box, were heated at 10 °C min^{-1} under N_2 gas flow up to 900°C. Raman spectra were recorded using a Raman spectrophotometer (LabRam HR-800, HORIBA Jobin Yvon) with 325 nm He–Cd laser.

Bulk densities of the powder-compressed pellets were calculated from the weight and volume of the pellets and relative densities were calculated by dividing the bulk density of the pellet by the apparent density of the obtained powder determined by an Ar gas pycnometer (AccuPyc II 1340, Shimadzu).

The elastic moduli were evaluated for the hot-pressed glass pellets by the ultrasonic pulse-echo technique using 5 MHz frequency transducers (5077PR, Olympus). Hot-pressed pellets were prepared by pelletizing the glass powders at 360 MPa at around each glass-transition temperature for 4 h in an Ar-filled glove box. The thickness and diameter of the prepared pellets were about 2 and 10 mm, respectively.

Electrical conductivities were measured for the samples pelletized under 720 MPa at room temperature. The pellets were 10 mm in diameter and about 1.5 mm in thickness. Gold electrode was deposited on both faces of the pellets by using a sputter apparatus (Quick Coater SC-701, Sanyu electron Corp.). Then stainless steel disks were attached to the pellets as current collectors. The prepared cell was sealed in a silica glass tube. Then AC impedance measurements were conducted under dry Ar gas flow using an impedance analyzer (SI-1260; Solartron analytical). The frequency range was 10 Hz to 8 MHz and the applied voltage was 50 mV. The AC impedance measurements were conducted at 25°C for the glass samples. Then the pellets were heated to above the crystallization temperatures to obtain glass-ceramics. The impedances of glass-ceramic samples were measured after cooling the pellets to 25°C. All the structural analyses and conductivity measurements were done in a dry Ar atmosphere without air exposure of the samples.

3. Results and discussion

The glass-forming region by twin-roller melt quenching was already reported for the pseudobinary system Li_3BO_3–Li_2SO_4.[8] Glass formation by the mechanochemical technique was tried for $x = 0$, 10, 25, 50, 60, 70, 80 and 90 of $(100 - x)Li_3BO_3 \cdot xLi_2SO_4$; all the compositions are the nominal ones. **Figure 1** shows the XRD patterns of the Li_3BO_3–Li_2SO_4 samples prepared by the mechanochemical technique for appropriate ball-milling periods of time; the milling period for each sample denoted in the figure was determined as an enough time to observe no diffraction peaks of starting materials. Halo patterns typical in amorphous materials are observed up to $x = 80$ prepared by 40–110 h milling of the mixture of Li_3BO_3 and Li_2SO_4 crystals, suggesting a very large glass-forming region in this system also in the case of mechanochemical process. The pattern of the $x = 90$ sample is similar to that of a high temperature phase, α-Li_2SO_4 (JCPDS#073-6539); somewhat peak shift to the higher angle side was observed and thus a α-Li_2SO_4-based solid-solution with Li_3BO_3 is formed at the composition.

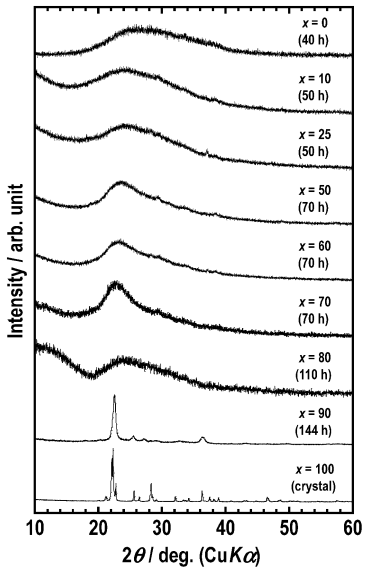

Fig. 1. XRD patterns of mechanochemically prepared $(100 - x)$-$Li_3BO_3 \cdot xLi_2SO_4$ samples and Li_2SO_4 crystal. Milling periods of time for each sample are noted in the bracket.

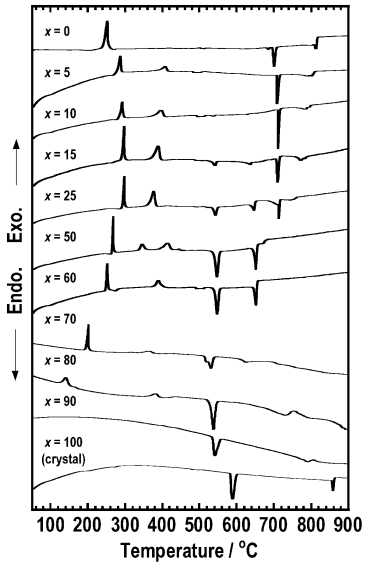

Fig. 2. DTA curves of the mechanochemically prepared $(100 - x)$-$Li_3BO_3 \cdot xLi_2SO_4$ samples and Li_2SO_4 crystal.

Figure 2 shows the DTA curves of the $(100 - x)Li_3BO_3 \cdot xLi_2SO_4$ ($x = 0$, 5, 10, 15, 25, 50, 60, 70, 80 and 90) samples prepared by the mechanochemical technique and crystalline Li_2SO_4 ($x = 100$). Since the amorphous samples tend to show small endothermic shifts typical of glass transition, these amorphous samples with $x = 0$–80 are considered as glassy materials. These glasses with $x = 0$–70 exhibit very sharp exothermic peaks. These exotherms are due to crystallization of these glasses because crystalline products are obtained after the heat treatments at temperatures beyond these exothermic peaks as shown later in **Fig. 6**.

Figure 3 shows the Raman spectra of mechanochemically prepared Li_3BO_3–Li_2SO_4 glasses. The Li_3BO_3 glass exhibits an intense band at around 930 cm^{-1}, which is assigned to the stretching mode of orthoborate BO_3^{3-} ions.[13] The Li_2SO_4 crystal exhibits an intense band at around 1010 cm^{-1}, which is assigned to the stretching mode of sulfate SO_4^{2-} ions.[14] The glasses containing both Li_3BO_3 and Li_2SO_4 show two bands near 930 and 1010 cm^{-1}. The 930 cm^{-1} band is weakened and the 1010 cm^{-1} band is strengthened with increasing the Li_2SO_4 content. Since there are no marked Raman bands other than these in any glass, these glasses contain no macroanions forming networks and consist only of Li^+ ions and discrete BO_3^{3-} and SO_4^{2-} ions. These glasses thus can be called as "ion glasses".

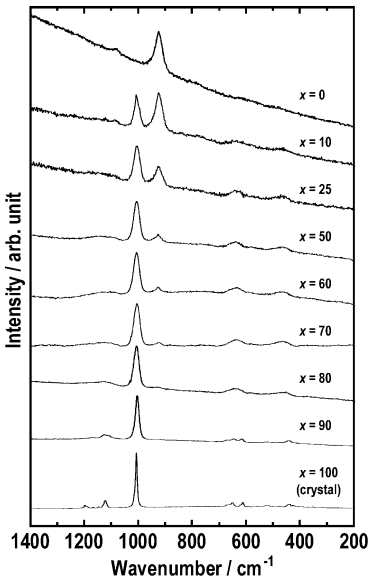

Fig. 3. Raman spectra of mechanochemically prepared $(100-x)$-$Li_3BO_3{\cdot}xLi_2SO_4$ samples and Li_2SO_4 crystal.

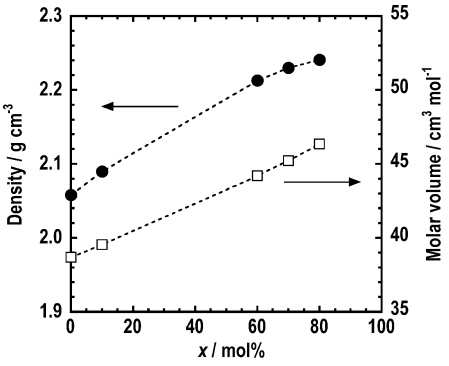

Fig. 4. Dependence of apparent density and molar volume on the Li_2SO_4 content of the $(100-x)Li_3BO_3{\cdot}xLi_2SO_4$ glasses.

Figure 4 shows the relationship between the apparent density of the obtained glass powder and the Li_2SO_4 content in the system $(100-x)Li_3BO_3{\cdot}xLi_2SO_4$. The density as well as its molar volume increases with increasing the Li_2SO_4 content, indicating that the addition of Li_2SO_4 instead of Li_3BO_3 brings a volume increase of the glass. The $(100-x)Li_3BO_3{\cdot}xLi_2SO_4$ glass powders were cold-pressed at 360 MPa and their relative densities were calculated. **Figure 5**(a) shows that with increasing the Li_2SO_4 content, the relative density increases linearly. Cross-sectional SEM images of the Li_3BO_3 ($x = 0$) and $20Li_3BO_3{\cdot}80Li_2SO_4$ ($x = 80$) glasses as shown in Figs. 5(b) and 5(c) also suggest that the glass is densified with the addition of Li_2SO_4. This change is probably brought by a larger molar volume of the glass with a higher amount of Li_2SO_4.

The $(100-x)Li_3BO_3{\cdot}xLi_2SO_4$ glasses were hot-pressed at around each glass-transition temperature to prepare further densified pellets and examine their elastic properties. The ultrasonic pulse-echo measurements were conducted for the hot-pressed pellets with the relative densities of 92–96% and the results are summarized in **Table 1**. The elastic moduli are roughly decreased with increasing the Li_2SO_4 content. This might be related to the molar volume of the glass. In typical oxide glasses, the elastic moduli decrease with increasing their mean atomic volumes.[15] Thus, the larger molar volume with increasing the Li_2SO_4 content (see Fig. 5) mainly contributes to the elastic modulus change.

Figure 6 shows the XRD patterns of the heat-treated Li_3BO_3–Li_2SO_4 glasses; the heat-treatment temperatures, ranging from 250 to 290°C, are just after the first sharp exothermic peaks in Fig. 2. The XRD patterns of the samples from $x = 5$–25 are attributable to solid solution phases of high temperature phase of Li_3BO_3 and Li_2SO_4. These phases are probably precipitated only from glass as metastable ones. In Fig. 2, several exothermic and endothermic peaks other than the first exothermic peaks due to crystallization are observed in the temperature range 300–900°C.

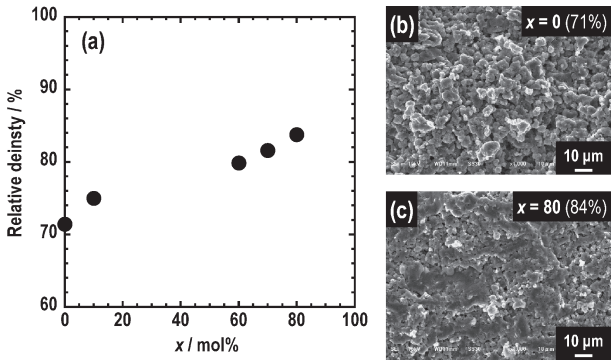

Fig. 5. (a) Relative density of the $(100-x)Li_3BO_3{\cdot}xLi_2SO_4$ glasses cold-pressed at 360 MPa. Cross-sectional SEM images of the (b) Li_3BO_3 ($x = 0$) and (c) $20Li_3BO_3{\cdot}80Li_2SO_4$ glasses.

Table 1. Molding temperature, bulk density, relative density, longitudinal velocity (V_L), shear velocity (V_S), shear modulus (G), Young's modulus (E), bulk modulus (K) and Poisson's ratio (ν) of the $(100-x)Li_3BO_3{\cdot}xLi_2SO_4$ glasses

Composition	Molding temperature /°C	Bulk density /g cm^{-3}	Relative density /%	V_L /m s^{-1}	V_S /m s^{-1}	G /GPa	E /GPa	K /GPa	ν
$90Li_3BO_3{\cdot}10Li_2SO_4$	240	1.92	91.8	6980	3180	19.4	53.1	67.6	0.37
$40Li_3BO_3{\cdot}60Li_2SO_4$	195	2.10	94.7	5760	2830	16.8	45.0	47.2	0.34
$30Li_3BO_3{\cdot}70Li_2SO_4$	160	2.13	95.7	6040	2820	17.0	46.2	55.2	0.36
$20Li_3BO_3{\cdot}80Li_2SO_4$	105	2.07	92.3	5530	2400	11.9	33.0	47.4	0.38

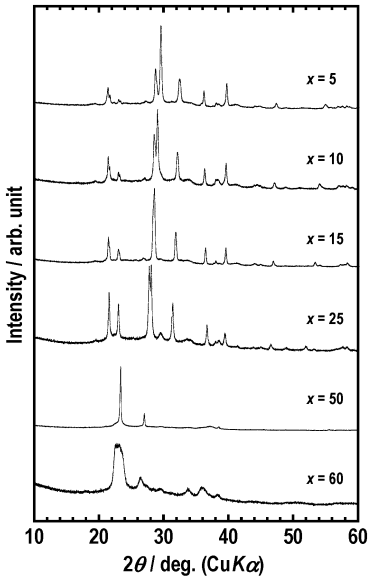

Fig. 6. XRD patterns of the heat-treated $(100-x)Li_3BO_3{\cdot}xLi_2SO_4$ glasses (glass-ceramics).

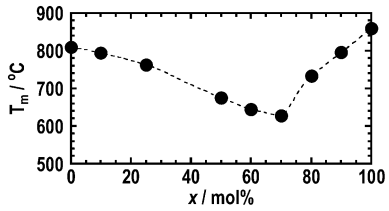

Fig. 7. Relationship between melting point and the Li_2SO_4 content in the $(100-x)Li_3BO_3{\cdot}xLi_2SO_4$ samples.

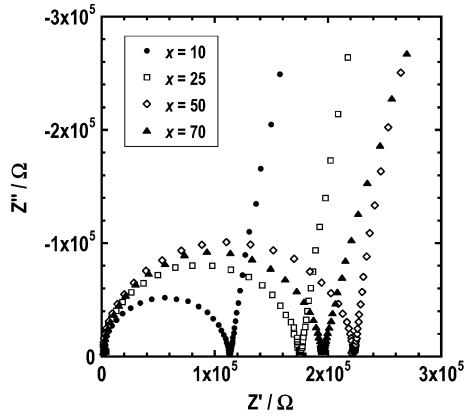

Fig. 8. Complex impedance plots of the $(100-x)Li_3BO_3{\cdot}xLi_2SO_4$ glasses at room temperature.

These DTA and XRD data suggest that the Li_3BO_3 crystal exhibit the melting temperature of 820°C and the liquidus temperature decreases from 820 to 630°C with increasing x from 0 to 70. Further increase of x increases the liquidus temperature toward the melting temperature of Li_2SO_4. **Figure 7** shows the relationship between melting point and the Li_2SO_4 content in the $(100-x)Li_3BO_3{\cdot}xLi_2SO_4$ samples. An eutectic composition should be around $x = 70$ and the eutectic temperature around 630°C.

Figure 8 shows the results of the complex impedance measurements of the Li_3BO_3–Li_2SO_4 glasses at room temperature as examples. These data were obtained for the glass powder-compressed pellets with blocking electrodes. The total impedance including bulk and grain boundary is attributed to the semicircle observed in all the glasses. The total resistance was obtained from the intersecting point of the semicircle with the real axis.

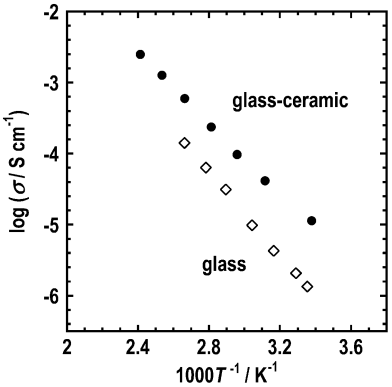

Fig. 9. Temperature dependence of electrical conductivity for the $90Li_3BO_3{\cdot}10Li_2SO_4$ ($x = 10$) glass and glass-ceramic.

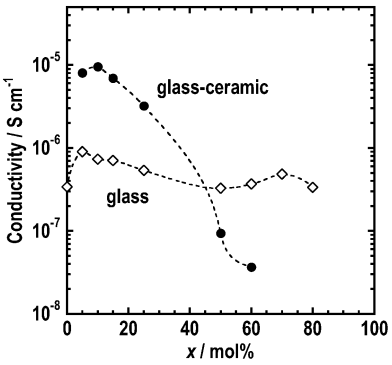

Fig. 10. Composition dependence of electrical conductivity at room temperature for the $(100-x)Li_3BO_3{\cdot}xLi_2SO_4$ glasses and glass-ceramics.

Figure 9 shows examples of the temperature dependence of electrical conductivity for the mechanochemically prepared $90Li_3BO_3{\cdot}10Li_2SO_4$ ($x = 10$) glass and the corresponding heat-treated sample (290°C), which is called as "glass-ceramic". The data are a good fit to the Arrhenius type equation. The conductivity at room temperature of the $90Li_3BO_3{\cdot}10Li_2SO_4$ glass-ceramic is one order of magnitude higher than that of corresponding glass. The activation energies for the glass and the glass-ceramic are calculated as 56 and 47 kJ mol^{-1}, respectively.

Figure 10 shows the composition dependence of ionic conductivity at room temperature for the cold-pressed Li_3BO_3–Li_2SO_4 glasses and glass-ceramics. The conductivity values of Li_3BO_3–Li_2SO_4 glasses range 10^{-7}–10^{-6} S cm^{-1} in whole the composition range. The increase of conductivity is observed with the addition of small amounts of Li_2SO_4. This would be due to the improvement of relative density of the cold-pressed pellet (see Fig. 5) in addition to the so-called "mixed-former effect".[16] Both effects of the relative density and the mixed-former probably come from the anion mixing in the glasses.

The glass-ceramics exhibits much higher room temperature conductivities around 10^{-5} S cm^{-1} with the composition range with $5 \leq x \leq 15$ compared to the corresponding glasses. Such a conductivity enhancement is attributable to the fact that the metastable solid solution phases of high temperature phase of Li_3BO_3 and Li_2SO_4[12] were precipitated in these glass-ceramic materials

as already shown in Fig. 6. The disappearance of the metastable phase at the compositions with $x \geq 50$ largely decreases the conductivity. Structural analyses of the metastable phases are important to determine the origin of the high conductivity of these glass-ceramics, and further investigation is needed to improve ionic conductivity of this type of oxides as high as that of sulfide-based solid electrolytes.

4. Conclusions

Low melting glasses in the system Li_3BO_3–Li_2SO_4 were obtained by the mechanochemical technique. These glasses had no network structure but consisted only of Li^+ ions and two discrete ortho-oxoanions of BO_3^{3-} and SO_4^{2-}; such glasses can be called "ion glass". The density and molar volume increased and elastic moduli decreased with an increase in the Li_2SO_4 content in the glasses. Ionic conductivity of the glasses was increased with an addition of small amounts of Li_2SO_4 to Li_3BO_3 in this system, which is probably due to the mixed-former effect and/or the improvement of relative density of the cold-pressed pellet. Highly conductive glass-ceramics were obtained by the heat treatment of the Li_3BO_3–Li_2SO_4 glasses, and exhibited higher ionic conductivities of about 10^{-5} S cm^{-1} at room temperature compared to the corresponding glasses. This conductivity enhancement by the heat treatment is probably due to the precipitation of solid solution phases with high temperature form of Li_3BO_3. Since the obtained glass-ceramics are low-melting, easily deformed and lithium ion conductive, these new "ion glass-ceramic" oxide electrolytes are promising for the application in all-solid-state oxide-based lithium batteries with high safety, reliability and stability.

References

1) K. Takada, *Acta Mater.*, 61, 759–770 (2013).
2) M. Ribes, B. Barrau and J. L. Souquet, *J. Non-Cryst. Solids*, 38–39, 271–276 (1980).
3) F. Mizuno, A. Hayashi, K. Tadanaga and M. Tatsumisago, *Adv. Mater.*, 17, 918–921 (2005).
4) Y. Seino, T. Ota, K. Takada, A. Hayashi and M. Tatsumisago, *Energy Environ. Sci.*, 7, 627–631 (2014).
5) N. Kamaya, K. Homma, Y. Yamakawa, M. Hirayama, R. Kanno, M. Yonemura, T. Kamiyama, Y. Kato, S. Hama, K. Kawamoto and A. Matsui, *Nat. Mater.*, 10, 682–686 (2011).
6) A. Sakuda, A. Hayashi and M. Tatsumisago, *Sci. Rep.*, 3, 2261 (2013).
7) M. Tatsumisago, N. Machida and T. Minami, *J. Ceram. Soc. Japan*, 95, 197–201 (1987).
8) M. Tatsumisago, H. Narita, T. Minami and M. Tanaka, *J. Am. Ceram. Soc.*, 66, C210–C211 (1983).
9) A. Hayashi, D. Furusawa, Y. Takahashi, K. Minami and M. Tatsumisago, *Phys. Chem. Glasses*, 54, 109–114 (2013).
10) M. He, H. Okudera, J. Fleig, A. Simon, X. L. Chen and J. Maier, *J. Solid State Chem.*, 178, 680–687 (2005).
11) E. A. Secco, *J. Solid State Chem.*, 96, 366–375 (1992).
12) M. Tatsumisago, R. Takano, K. Tadanaga and A. Hayashi, *J. Power Sources*, 270, 603–607 (2014).
13) W. L. Konijnendijk and J. M. Stevels, *J. Non-Cryst. Solids*, 18, 307–331 (1975).
14) K. Nakamoto, "Infrared and Raman spectra of inorganic and coordination compounds", 3rd ed., Wiley, New York (1978).
15) K. Takahashi and A. Osaka, *J. Ceram. Soc. Japan*, 91, 116–120 (1983).
16) B. Raguenet, G. Tricot, G. Silly, M. Ribes and A. Pradel, *Solid State Ionics*, 208, 25–30 (2012).